Biomaterials 34 (2013) 3324–3335

Contents lists available at SciVerse ScienceDirect

Biomaterials

journal homepage: www.elsevier.com/locate/biomaterials

The promotion of a functional fibrosis in skeletal muscle with volumetric muscle loss injury following the transplantation of muscle-ECM

Benjamin T. Corona, Xiaowu Wu, Catherine L. Ward, Jennifer S. McDaniel, Christopher R. Rathbone, Thomas J. Walters*

US Army Institute of Surgical Research, Extremity Trauma and Regenerative Medicine, 3698 Chambers Pass, Fort Sam Houston, TX 78234, USA

ARTICLE INFO

Article history:
Received 15 November 2012
Accepted 11 January 2013
Available online 4 February 2013

Keywords:
Muscle
ECM (extracellular matrix)
Transplantation
Fibrosis
Trauma
VML (volumetric muscle loss)

ABSTRACT

Tissue engineering strategies that primarily use biological extracellular matrices (ECMs) with or without the inclusion of a stem or progenitor cell source are under development for the treatment of trauma resulting in the loss of a large volume of skeletal muscle (i.e., volumetric muscle loss; VML). The explicit goal is to restore functional capacity to the injured tissue by promoting generation of muscle fibers. In the current study, a syngeneic muscle-derived ECM (mECM) was transplanted in a rat tibialis anterior (TA) muscle VML model. Instead of muscle fiber generation a large fibrotic mass was produced by mECM transplantation out to six months post-injury. Surprisingly, recovery of one-third of the original functional deficit was still achieved by two months post-injury following mECM transplantation. These counterintuitive findings may be due, at least in part, to the ability of mECM to attenuate muscle damage in the remaining muscle as compared to non-repaired muscle. These findings point to a novel role of biological ECMs for the treatment of VML, wherein the remaining muscle mass is protected from prolonged overload injury.

Published by Elsevier Ltd.

1. Introduction

Skeletal muscle has a remarkable capacity to self-repair, regenerate, and remodel in response to injury and stress. Rodent muscle injury models in which satellite cells remain viable [1,2], the basement membrane is left relatively intact [3,4], and an appropriate inflammatory response ensues [5,6] are generally fully recoverable following ~1–2 months of healing. However, in man [7,8] and rodents [9–14], trauma that results in the frank loss of a large volume of skeletal muscle tissue (i.e., volumetric muscle loss; VML) cannot be completely regenerated under endogenous mechanisms. The chronic loss of muscle mass and function can lead to a cycle of untoward clinical outcomes manifesting in mandatory or elected amputation and/or disablement [8,15]. Since the seminal papers of Studitsky [16] and Carlson [17–19] demonstrated the capacity of skeletal muscle to regenerate following severe trauma over 50 years ago, many of the molecular and cellular mechanisms regulating regeneration have been elucidated. However, only modest gains have been made towards developing clinical therapies that promote generation of a large volume of muscle after severe trauma or surgical excision.

Skeletal muscle tissue engineering therapies may provide an unprecedented treatment option for volumetric muscle loss. Currently, many tissue engineering approaches involve transplantation of a sheet of decellularized extracellular matrix (ECM) either with or without the inclusion of a stem or progenitor cell source [9,10,20–24]. In fact, to date a scaffold composed of laminated sheets of porcine derived small intestinal submucosa (SIS) ECM is the only FDA-approved tissue engineering device reported to treat volumetric muscle loss (~3 years post-injury) in the clinic [8]. The use of biological decellularized matrices is based upon the *de novo* role of muscle ECM following injury. That is, transplanted biological ECMs are degraded in the presence of a targeted immune response [25,26]. The degradation products are thought to present biological factors and structures (e.g., growth factors, cryptic peptides, basement membrane fragments) that interact with the host to create a pro-regenerative environment [3,23,25,27,28]. As a result, transplantation of a variety of ECMs in preclinical animal models has resulted in modest levels of muscle fiber generation at the site of the defect during the initial months post-injury [20,28–30]. However, an apparent enhanced rate of muscle fiber generation at

* Corresponding author. Tel.: +1 210 916 2726; fax: +1 210 916 3877.
E-mail addresses: thomas.walters@us.army.mil, dr.thomas.walters@gmail.com (T.J. Walters).

0142-9612/$ – see front matter Published by Elsevier Ltd.
http://dx.doi.org/10.1016/j.biomaterials.2013.01.061

Report Documentation Page

Form Approved
OMB No. 0704-0188

1. REPORT DATE	2. REPORT TYPE	3. DATES COVERED
01 APR 2013	**N/A**	**-**

4. TITLE AND SUBTITLE	5a. CONTRACT NUMBER
The promotion of a functional fibrosis in skeletal muscle with volumetric muscle loss injury following the transplantation of muscle-ECM	5b. GRANT NUMBER
	5c. PROGRAM ELEMENT NUMBER
6. AUTHOR(S)	5d. PROJECT NUMBER
Corona B. T., Wu X., Ward C. L., McDaniel J. S., Rathbone C. R., Walters T. J.,	5e. TASK NUMBER
	5f. WORK UNIT NUMBER
7. PERFORMING ORGANIZATION NAME(S) AND ADDRESS(ES)	8. PERFORMING ORGANIZATION REPORT NUMBER
United States Army Institute of Surgical Research, JBSA Fort Sam Houston, TX	
9. SPONSORING/MONITORING AGENCY NAME(S) AND ADDRESS(ES)	10. SPONSOR/MONITOR'S ACRONYM(S)
	11. SPONSOR/MONITOR'S REPORT NUMBER(S)

12. DISTRIBUTION/AVAILABILITY STATEMENT
Approved for public release, distribution unlimited

13. SUPPLEMENTARY NOTES

14. ABSTRACT

15. SUBJECT TERMS

16. SECURITY CLASSIFICATION OF:			17. LIMITATION OF ABSTRACT	18. NUMBER OF PAGES	19a. NAME OF RESPONSIBLE PERSON
a. REPORT	b. ABSTRACT	c. THIS PAGE			
unclassified	**unclassified**	**unclassified**	**UU**	**12**	

later times post-injury (4–6 months) has been reported in the dog hindlimb [22], indicating that in large, and potentially small, mammals a prolonged post-operative period is required to realize the regenerative potential of biological ECM devices.

Volumetric muscle loss has been defined as "the traumatic or surgical loss of skeletal muscle with resultant functional impairment" [15]. Therefore, a successful tissue engineering therapy for VML is one that restores functional capacity to the injured musculature. Ideally, transplantation of a biological ECM (with or without the inclusion of stem or progenitor cells) at the site of VML will enable generation of functional muscle fibers to replace those that were lost. At the same time, it is plausible that such treatments could also have a therapeutic impact on the remaining muscle mass leading to additional improvements in functional capacity; however, no study has explicitly studied these effects.

The purpose of the current study is two-fold: First, we sought to determine if the transplantation of a syngeneic muscle derived ECM (mECM) promotes functional recovery in a Lewis rat tibialis anterior muscle (TA) VML model [14] over the first six months post-injury. Second, upon observing a significant improvement in functional capacity with mECM transplantation, we sought to determine the general mechanism (muscle fiber generation vs. regeneration of the remaining muscle) by which the mECM improved function.

2. Methods

2.1. Animals

This study has been conducted in compliance with the Animal Welfare Act, the Implementing Animal Welfare Regulations and in accordance with the principles of the Guide for the Care and Use of Laboratory Animals. All animal procedures were approved by the United States Army Institute of Surgical Research Animal Care and Use Committee. Adult Male Lewis rats (Harlan Laboratories, Indianapolis, IN) were housed in a vivarium accredited by the American Association for the Accreditation of Laboratory Animal Care and provided with food and water ad libitum.

2.2. Preparation and characterization of muscle-derived ECM (mECM)

2.2.1. Source and decellularization procedure

TA muscles were isolated from donor Lewis rats. The tendon and fascia were removed and TA muscle decellularization was performed using an enzymatic and detergent-based method previously described for rat skeletal muscle [31] with some modifications. Briefly, TA muscles were frozen at −20 °C and then soaked in dH_2O or Dulbecco's Modified Eagle Medium (DMEM; Invitrogen, Carlsbad, CA) for 72 h at 4 °C. The muscles were then treated with 0.15% trypsin in DMEM (Invitrogen, Carlsbad, CA) at room temperature for 1 h, after which the enzyme was neutralized with 10% fetal bovine serum (FBS) in DMEM overnight at 4 °C. Next, the muscles were treated with 3.0% triton x-100 (Fisher Scientific, Pittsburg, PA) solution until the muscle was clear (2 changes per day; 3–5 days), followed by rinses in dH_2O or PBS for three days (2–3 changes per day). All mECMs were sterilized with UV light for at least 4 h.

2.2.2. Genomic DNA quantification

Genomic DNA extraction and quantification were performed in three mECMs that were dissected into proximal, medial, and distal sections. Genomic DNA was isolated using TRIzol Reagent® (Invitrogen, CA, USA) following manufacturer's instructions. Rat TA muscle not subjected to the decellularization process was used as a control. Briefly, TRIzol Reagent® was added to each sample followed by power homogenization (Bio-Gen PRO200, CT, USA) and phenol-chloroform separation. DNA was precipitated with ethanol, washed with sodium citrate in ethanol and resuspended in 8 mM NaOH. DNA samples were quantified using a Nanodrop 8000 (Thermo Scientific, DE, USA) and normalized to initial sample weight.

2.2.3. In vitro cell proliferation assay

Tissue culture plates (48-well) were coated in 0.2 mg/mL collagen (Becton Dickinson, Rat Tail Collagen I) dissolved in 1% acetic acid, were incubated for 1 h at room temperature, and were then washed with phosphate buffered saline (PBS) prior to cell seeding. Rat satellite cells were isolated from hindlimb muscles similar to that previously described by Allen et al., [32], and were seeded at approximately 3000 cell/cm^2 in growth media (DMEM + 20% FBS + 1% Antibiotic Antimycotic) and attached for 24 h. Control wells with no cells were also plated with media. After attachment, media was removed and replaced with media containing either 10% fetal bovine serum (FBS) or 10% horse serum (HS). Treatment groups included control media and media supplemented with 0.5 mg/mL mECM. A CyQUANT® cell proliferation assay was performed according to the manufacturer's instructions (Life Technologies™) on days 0, 1, 3, and 5 ($n = 4$ wells per treatment group at each time point). Plates were read on a SpectraMax M2 plate reader (Molecular Devices). Background was diminished by subtracting appropriate blank controls for each group. For these studies, mECM was frozen, lyophilized, and then milled using a Thomas Wiley Mini-Mill (Thomas Scientific) and passed through a number 20 mesh (~841 μm).

2.3. Bone marrow-derived mesenchymal stem cell isolation and characterization

To isolate bone marrow-derived stem cells, both the proximal and distal epiphysis of isolated tibiae and femurs of male Lewis rats were removed using a Boehier bone cutter. The medullary cavity was flushed two times with Hank's Balanced Salt Solution (HBBS) using a 10 mL syringe and 20-gauge needle, and the bone marrow cell suspension centrifuged for 5 min at 500× g at room temperature. The cell pellet was re-suspended in growth medium. Cells were seeded (5×10^5 cells/cm^2) on 25 cm^2 culture flasks, the nonadherent cells removed after 2 days, and adherent cells cultured until colonies reached 80–90% confluence (~2 weeks). At the first and subsequent passages, cells were detached using 0.05% trypsin-EDTA, centrifuged at 500 g for 5 min, and seeded at 40,000/cm^2 in a 75 cm^2 culture flasks. Cells from passage 4–6 were used in this study. All culture reagents were purchased from Invitrogen (Grand Island, NY).

To verify the purity of the BMSC isolation, a subset of cells were used for flow cytometry analysis. Cells detached from culture flasks were washed with staining buffer (BioLegend, San Diego, CA) three times and incubated with Alexa 488 or PE-conjugated anti-CD90, CD29, CD54, CD44H, CD45, or CD34 (all from BioLegend, San Diego, CA) monoclonal antibodies or FITC or PE-conjugated nonspecific IgG antibodies for negative controls for 40 min at 4 °C. After three washes in staining buffer, cells were centrifuged (500× g), the cell pellet resuspended in 100 μL volume of cell staining buffer (BioLegend), and flow cytometry analyses performed using a FACAria flow cytometer (Becton–Dickinson, Mt, View, CA). Ten to fifty thousand cells were analyzed using FACSDiva software (BD Biosciences, Mt, View, CA). The percent positive staining for each marker was: CD90, 76.8%; CD29, 99.5%; CD54, 92.0%; CD44H,98.3%; CD34,0%; and CD45, 0.4%.

2.4. VML injury model

The surgical procedure for creating VML in the rat TA muscle was performed as described previously [14]. Using aseptic technique, a surgical defect of ~10× 7 × 3 mm (length × width × depth) was created in the middle third of the TA muscle using a scalpel. The excised defect weight approximated ~20% of the estimated TA muscle weight.

2.5. TA muscle VML repair

Immediately after the creation of the muscle defect, mECM was placed into the defect area and sutured to the remaining TA muscle at the corners and margins of the implant using prolene suture (6–0). Care was taken to include the epimysium of the TA muscle in the suture, as this suturing method withstands tension well and thus promotes superior suture retention [33]. Additionally, these sutures were used as markers of the defect implant interface at the time of harvest. Seven days after injury, a longitudinal skin incision was made over superficial aspect of the TA muscle. Either saline or saline + BMSCs (1×10^6 cells in 30 μL) was injected into the mECM using an insulin syringe. The skin was closed with simple interrupted prolene suture (6–0).

2.6. In vivo functional analysis

Anterior crural muscle *in vivo* mechanical properties were measured in anesthetized rats (isoflurane 2–2.5%) in both legs, following EDL muscle distal tenotomy using methodology we have described previously [14]. Core body temperature was monitored and maintained at 36–37 °C. A nerve cuff was implanted in each leg around the peroneal nerve. The foot was strapped using silk surgical tape to a foot plate attached to a dual-mode muscle lever system (Aurora Scientific, Inc., Mod. 305b). The knee was secured on either side using a custom-made mounting system, and the knee and ankle were positioned at right angles. Then, a skin incision was made at the antero-lateral aspect of the ankle and the distal EDL muscle tendon was isolated and severed above the retinaculum. The TA muscle and tendon, as well as the retinaculum were undisturbed. Peak isometric torque was determined by stimulating the peroneal nerve using a Grass stimulator (S88) at 150 Hz with a pulse-width of 0.1 ms across a range of voltages (2–8 V).

2.7. In situ functional analysis

In situ muscle mechanical properties were measured as previously described [34,35]. A sub-population of non-repaired VML injured muscle forces at two and four months post-injury were reported on previously [14]. To control for normal growth and differences among groups (Table 1), forces were normalized to body weight. The transected common peroneal nerve was stimulated via a nerve cuff electrode using a pulse stimulator (A-M Systems, Inc, Mod. 2100). The distal tendon

Table 1
Morphological and functional characteristics.

	Uninjured			VML − no repair			VML-mECM			VML-mECM & BMSC		
	Post-injury (months)			Post-injury (months)			Post-injury (months)			Post-injury (months)		
	2	4	6	2	4	6	2	4	6	2	4	6
Sample size (n)	19	23	23	3	7	10	8	8	5	8	8	8
Body weight at surgery (g)	–	–	–	348 ± 3	344 ± 3	357 ± 2	344 ± 6	343 ± 8	340 ± 8	339 ± 3	344 ± 7	338 ± 6
Body weight at sacrifice (g)	–	–	–	493 ± 8	493 ± 6	524 ± 5	430 ± 10†	482 ± 14	505 ± 7	410 ± 6†	468 ± 10	486 ± 8†
TA muscle defect wt (mg)	–	–	–	101 ± 2	101 ± 2	112 ± 5	111 ± 5	102 ± 2	100 ± 1	102 ± 2	109 ± 5	99 ± 3
TA muscle weight (mg)	691 ± 13	728 ± 11	742 ± 20	606 ± 40*	643 ± 20*	712 ± 21	655 ± 25	702 ± 23†	693 ± 23	609 ± 8*	709 ± 22†	701 ± 17
TA weight (mg): body weight (g)	1.60 ± 0.02	1.52 ± 0.02	1.47 ± 0.03	1.23 ± 0.06*	1.31 ± 0.04*	1.36 ± 0.04	1.52 ± 0.05†	1.47 ± 0.06†	1.37 ± 0.05	1.49 ± 0.01*†	1.52 ± 0.06†	1.44 ± 0.02
P_o (N/kg body wt)	27.4 ± 0.8	26.3 ± 0.4	25.1 ± 0.5	18.6 ± 0.2*	18.4 ± 1.4*	19.8 ± 0.6*	21.1 ± 0.9*†	20.0 ± 0.8*†	19.6 ± 0.7*	21.3 ± 0.6*†	20.9 ± 1.2 *†	20.6 ± 0.8*
L_o (mm)	32.2 ± 0.3	33.1 ± 0.4	33.2 ± 0.3	31.7 ± 0.7	32.4 ± 0.4	33.5 ± 0.4	32.7 ± 0.6	32.5 ± 0.4	32.3 ± 0.4	32.2 ± 0.4	33.9 ± 0.6	32.6 ± 0.3

Values are means ± SEM. P_o, peak isometric tetanic torque; L_o, optimal muscle length. Superscripts: * ≠ uninjured, † ≠ no repair within a given time point post-injury ($p < 0.05$).

of the tibialis anterior (TA) was isolated and cut. The distal 1/3 of the TA was dissected free from the surrounding musculature gently leaving the origin and neurovascular pedicle intact. The distal tendon was threaded through a hole in the lever arm of a dual-mode servo muscle lever system (Aurora Scientific, Inc., Mod. 309b) and secured with 4–0 silk suture. The lower leg was secured and stabilized with pins at the knee and ankle joints. Core body temperature was monitored and maintained at 36–37 °C. All measurements were made with the muscles set at optimal length (L_o) with a 0.1 ms pulse width at a voltage corresponding to 1.5–2× the voltage required for peak twitch tension (P_t). L_o was determined from P_t using an automated routine as follows: starting in a slack position the muscle was stimulated at 1 Hz for a set of 8 twitches; the last two twitches were averaged and the P_t was stored. The lever then automatically moved 0.1 mm, and the routine was repeated 2 s later. Each twitch set including lever movement took 10 s. This continued until the average P_t did not change by more than 2% between 3 consecutive twitch sets, indicating the plateau of the isometric length–tension curve. Optimal length (L_o) was defined as the second of the three twitch sets. Following establishment of L_o, peak tetanic isometric force was measured with a 400 ms train over a range of frequencies (100–200 Hz). A custom, LabView™ (National Instruments Inc.) based program was used to control the muscle lever systems and collect, store and analyze the data from *in vivo* and *in situ* muscle function studies.

2.8. TA muscle harvest and histological procedures

TA muscles were embedded in a talcum-based gel and frozen in 2-methylbutane (Fisher Scientific) supercooled in liquid nitrogen. Cryostat cross-sections (8 μm) were cut from the middle third of the TA muscle in the area where the original surgical defect was made. Sections were stained with hematoxylin and eosin (H&E). Immunofluorescence stained tissue sections were probed for collagen I (1:500, Millipore AB755P), sarcomeric myosin (MF20: 1:10, Hybridoma Bank), laminin (1:200, Abcam AB11575), CD68 (1:50, AbD Serotec MCA341R), cellular membranes (wheat germ agglutinin; WG: 1:20, Invitrogen), and nuclei (DAPI; 1:100, Invitrogen). Sections were blocked in PBS containing 0.05% Tween 20, 5% goat serum, and 0.1% bovine serum for 1 h at room temperature and then incubated in primary antibody solutions overnight at 4 °C. Sections were washed in PBS and incubated in corresponding Alexaflour 488 or 596 labeled secondary antibodies (1:200–1:500, Invitrogen) at room temperature for 1 h. The sections were then stained with DAPI and mounted in Fluoromount (Fisher Scientific). Qualitative assessments were made by observing three sections (separated by no less than 160 μm) from 3 to 5 muscles per time point per group. CD68 + cells were counted in mECM-repaired and no repair tissue at two weeks post injury. Five high-powered fields (400× magnification) from a section from the middle of the defect from three muscles per experimental group were analyzed. At two months post-injury, the area fraction of fibrous tissue within the remaining muscle mass was determined from collagen I stained sections of uninjured and VML no repair, mECM-repaired, and mECM + BMSCs-repaired muscles (n = 3 muscles, 3–5 non-overlapping 200× images per muscle). Images were converted to 8-bit, background subtracted and rescaled from 0 to 255 before a threshold was applied to each image using Image J (NIH, Bethesda, MD).

2.9. Muscle fiber cross sectional area analysis

Fiber cross-sectional area was determined using a custom-written macro in Image J (NIH, Bethesda, MD), using methodology described in Meyer and Lieber [36]. Images captured from the remaining muscle mass of laminin stained sections (n = 5–9 muscles per group; ~2000 fibers per group) were analyzed. Only fibers with sizes between 50 and 6000 μm^2 and a circularity between 0.3 and 1.0 were included for analysis to remove the measurement of neurovascular bundles, optically fused fibers, and oblique fibers [36]. Fibers on the border of the image were also excluded from analysis.

2.10. Statistics

Cellular, morphological and functional data were initially analyzed using separate ANOVAs. Upon finding significance, post-hoc means comparisons were performed using Fisher's LSD. Statistical significance was achieved at an alpha of 0.05. Statistical analyses were performed using SPSS 18.0.

3. Results

3.1. In vitro characterization of mECM

mECMs were decellularized from whole rat TA muscles using an enzymatic and detergent-based approach as described in the methods (Fig. 1A). mECMs were found to be devoid of nuclei as determined by DAPI staining (Fig. 1B). The DNA content found within mECMs averaged less than 6 ng/mg mECM (Fig. 1C), values well-below that of native skeletal muscle and the criteria

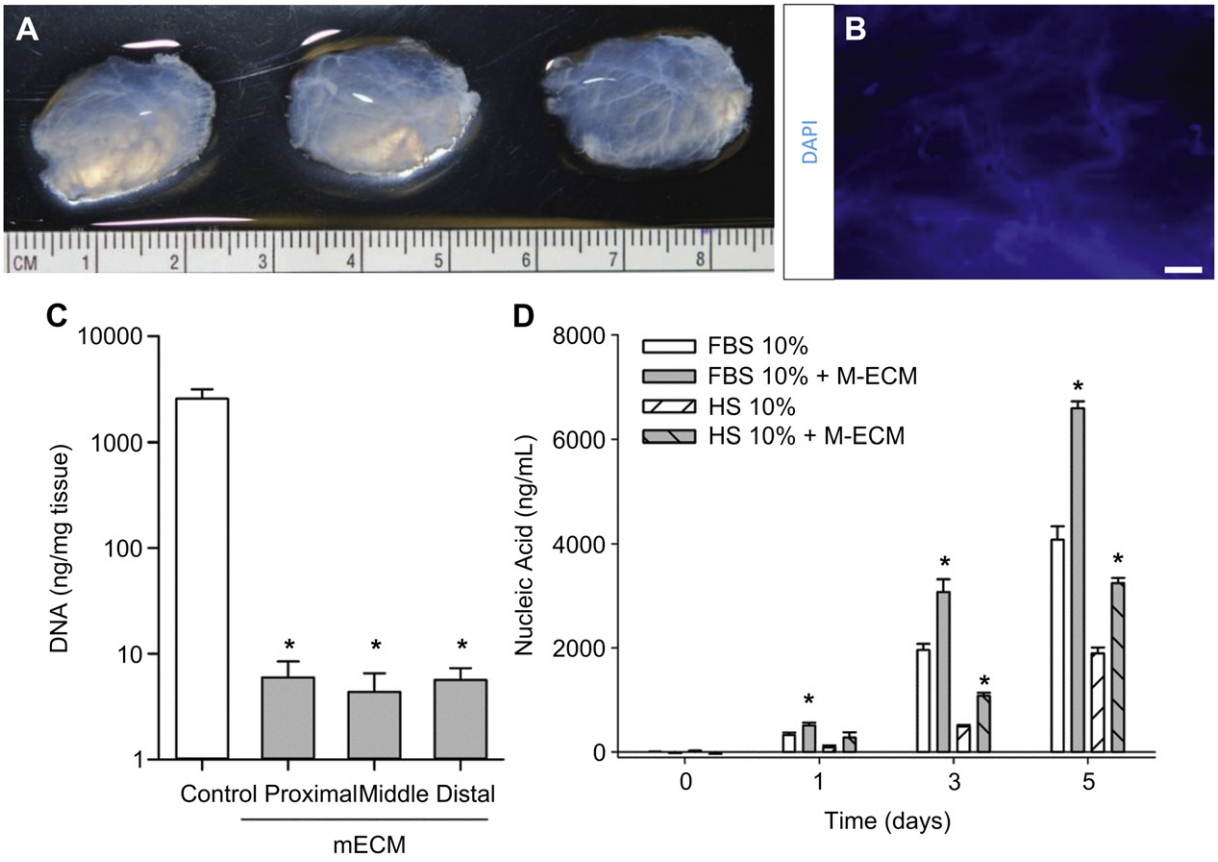

Fig. 1. mECM morphology and characterization. (A) Gross morphology of mECMs prior to transplantation. (B) DAPI staining of a thin slice of mECM demonstrating the removal of nuclei. Scale bar = 200 μm (C) DNA content of mECM; *less than native muscle (control) $p < 0.05$. (D) Cell proliferation in the presence and absence of mECM in 10% FBS or HS; *greater than respective serum control at the time point specified $p < 0.05$. Values are means ± SEM.

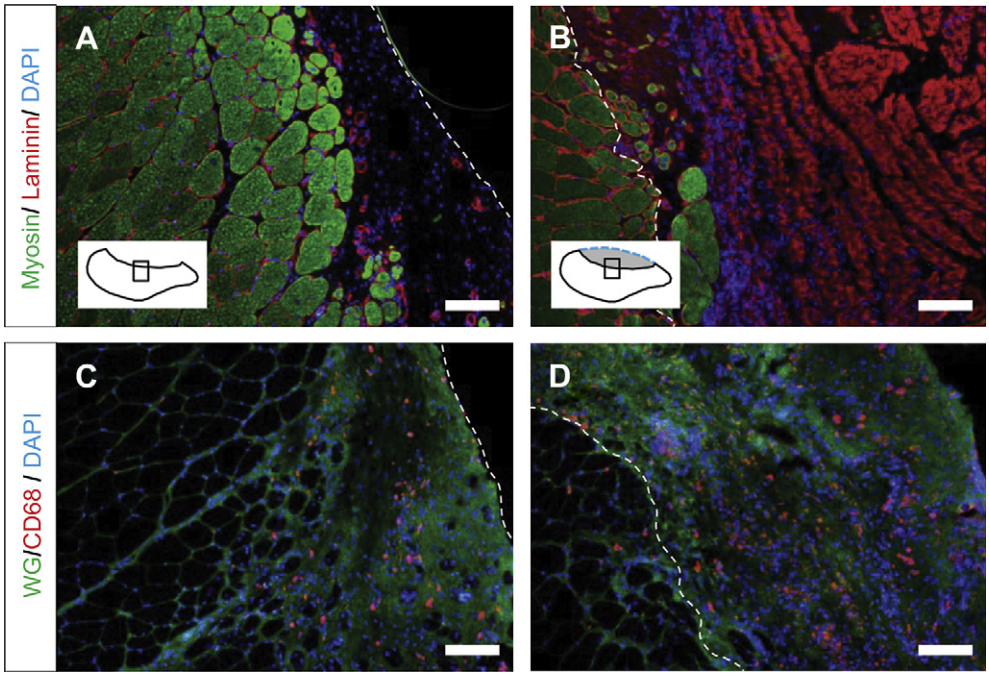

Fig. 2. Acute regenerative host response to volumetric muscle loss with and without transplantation of homologous mECM. Non-repaired (A & C) and mECM-repaired (B & D) TA muscles were harvested two weeks post-injury and cross-sections of the muscle were fluorescently probed for markers, as denoted on each row of images and described in the methods. *Note*: The diagram of the TA muscle illustrates where the depicted images for each group were captured relative to the defect site. White dashed lines indicate the approximate interface between the remaining muscle mass (left) and transplanted mECM (right). Images are of 100× magnification; Scale bar = 100 μm.

(<50 ng/mg) of a sufficiently decellularized ECM [37]. Moreover, mECM fragments were found to enhance satellite cell proliferation *in vitro* in a higher (FBS) and lower (HS) nutrient-rich media (Fig. 1D), indicating that while the mECM was decellularized, biological components capable of promoting cell proliferation remained present.

3.2. Early response after VML & mECM repair

Two weeks after injury very little myogenesis, as indicated by the presence of small myosin positive fibers, were observed in non-repaired and mECM repaired muscles (Fig. 2A and B). Macrophages (CD68 + cells) were localized within the remaining muscle mass, which appeared fibrotic, in non-repaired tissues, but were primarily localized within the transplanted mECM (Fig. 2C and D). The magnitude of the immune (CD68 + cells) response was greater with mECM transplantation than with no-repair (73 ± 7 vs. 26 ± 4 CD68 + cells per 400× high powered field, respectively; $p < 0.001$). Interestingly, muscle fiber damage, marked by inflammation and focal sites of muscle fiber necrosis, was observed in the remaining muscle mass (*in discrete areas from the defect site*) of mECM-repaired and to a qualitatively greater extent in the non-repaired tissue (Fig. 3). In response to the frank loss of ~20% of muscle mass and potentially the ensuing damage to the remaining tissue, an ~30% isometric torque deficit was observed two weeks post-injury for non-repaired and mECM-repaired muscles (Fig. 4).

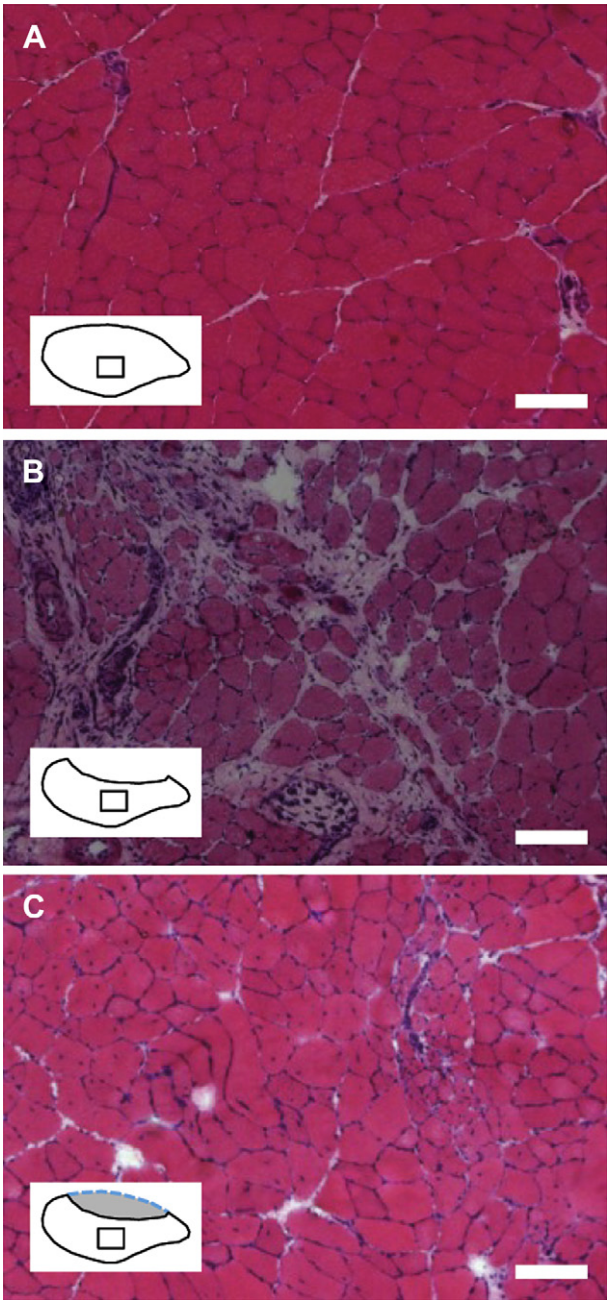

Fig. 3. Muscle fiber damage in the remaining muscle mass two weeks after volumetric muscle loss with and without transplantation of homologous mECM. Cross-sections of uninjured (A), non-repaired (B), and mECM-repaired (C) VML injured muscles were stained with hematoxylin and eosin. *Note*: The diagram of the TA muscle illustrates where the depicted images for each group were captured relative to the defect site. Images are of 100× magnification; Scale bar = 100 μm.

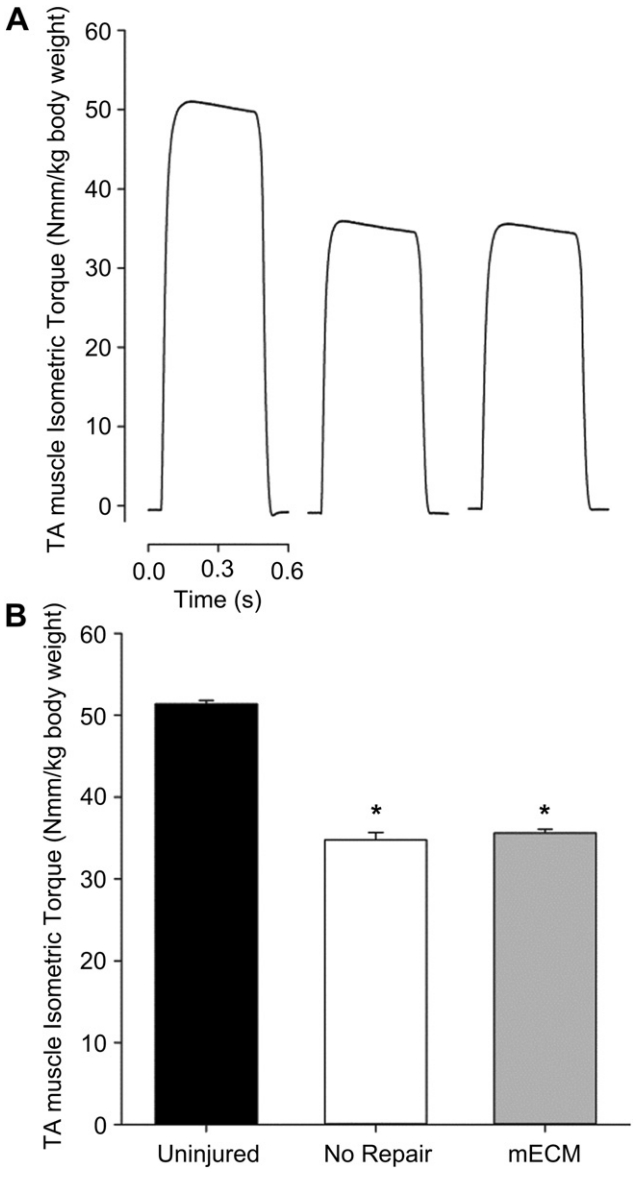

Fig. 4. *In vivo* TA muscle isometric torque two weeks after volumetric muscle loss. Isometric torque was measured in age-matched uninjured, non-repaired, and mECM-repaired TA muscles following stimulation of the common peroneal nerve (0.1 ms pulse width; 150 Hz; 400 ms train; 2–5 V). Representative torque tracings for each group (A) and group means ± SEM ($n = 3$/group; B) are presented. *group means are statistically different ($p < 0.05$) from uninjured muscle.

3.3. Prolonged tissue generation after mECM repair

3.3.1. Myogenesis after mECM transplantation

In line with the low myogenic response observed at two weeks, limited evidence of muscle fiber generation (i.e., myosin + fibers) within the area of the transplanted mECM was observed out to six months post-injury (Fig. 5A, C, & E). In an effort to augment the myogenic regenerative phenotype within the defect, BMSCs were injected into the mECM seven days after implantation. This approach was chosen because mesenchymal stem cells have been shown to differentiate along a myogenic lineage in response to appropriate mechanical and environmental cues [38], to migrate to otherwise healthy muscle in response to injury [39], and even to enhance the functional restoration of skeletal muscle following crush [40] and volumetric muscle loss [21] injuries. In general, the delayed injection of BMSCs resulted in the generation of a similarly small volume of muscle fibers at the interface with the native tissue as observed with mECM alone (Fig. 5B, D, F).

Specifically, over the first six months post-injury the following observations were made after mECM transplantation with or without the delivery of BMSCs: At two months post-injury there were signs of small muscle fibers within the defect, however, the fibers were located only ~100 μm from the remaining musculature and did not visibly approximate the cross-sectional area of mature muscle fibers. At four months, the fate of the putatively early developing fibers was not apparent suggesting that either the fibers did not survive or they merged with the remaining musculature. In support of the latter possibility, in some instances with either treatment group a band of muscle fibers (e.g., 3 to 4 fibers) was observed and they were oriented perpendicular to the muscle fibers in the remaining muscle mass. At six months post-injury, we did not observe overt signs of delayed muscle fiber generation in TA muscles with either treatment, i.e., no small muscle fibers were observed within the defect area. Instead, at four and six months post-injury adipocytes (confirmed with oil red o staining, data not shown) accumulated near the interface with the remaining muscle

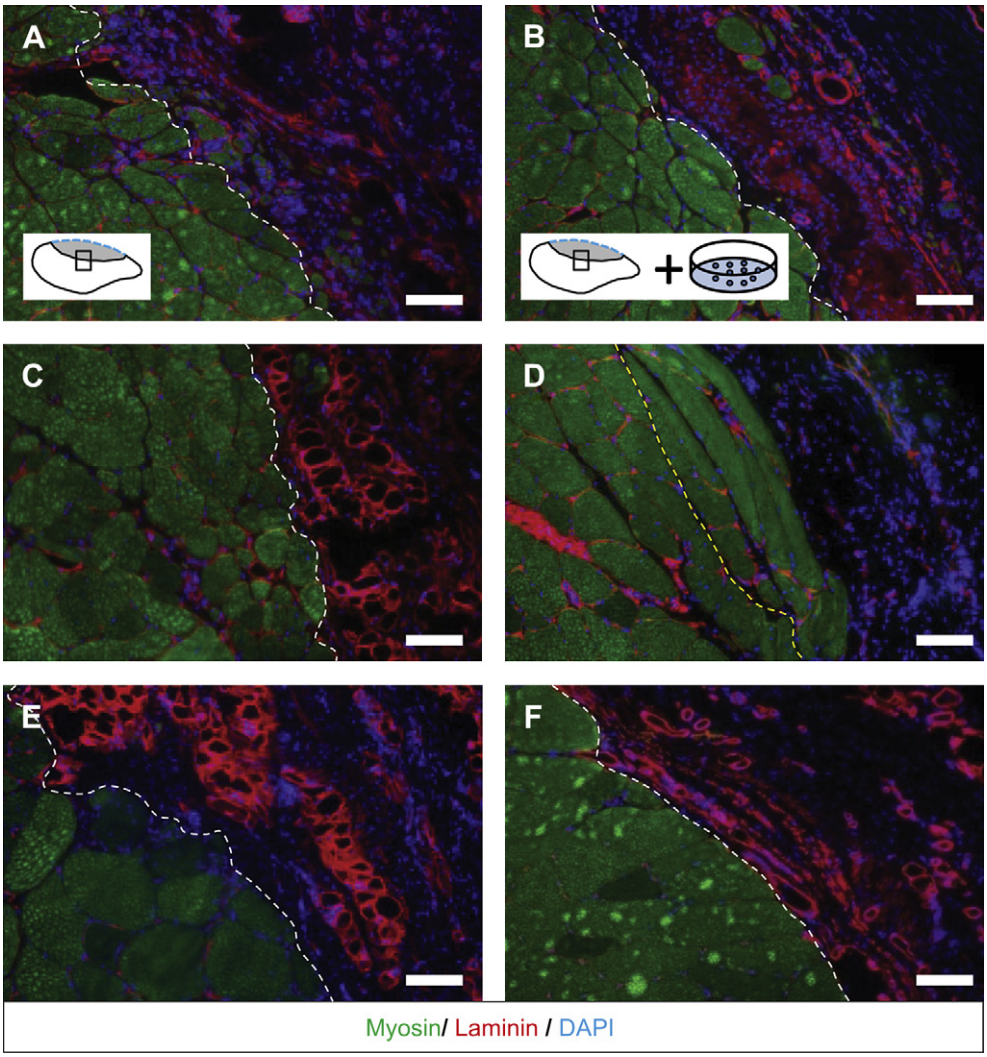

Fig. 5. Characterization of muscle fiber generation at the defect area out to six months after VML injury in muscles repaired using tissue engineering strategies. Injured muscles were repaired with mECM (A, C, & E) or mECM with the delayed addition of ~1 million BMSCs directly to the mECM 7 days post-injury (B, D, & F). TA muscles were harvested at 2 (A & B), 4 (C & D), and 6 (E & F) months post-injury and cross-sections were probed for sarcomeric myosin, laminin, and nuclei (DAPI). *Note*: The diagram of the TA muscle illustrates where the depicted images for each group were captured relative to the defect site. Dashed lines indicate the approximate interface between the remaining muscle mass (left) and transplanted mECM (right). In some cases for mECM and mECM + BMSC groups, longitudinal fibers were observed in close proximity to the remaining muscle mass (D; Yellow dashed line). Images are of 100× magnification; Scale bar = 100 μm. (For interpretation of the references to color in this figure legend, the reader is referred to the web version of this article.)

mass (e.g., Fig. 5C, E, & F). Collectively, limited signs of *de novo* muscle fiber generation were observed following transplantation of mECM with or without injection of BMSCs.

3.3.2. Fibrosis after VML in non-repaired and mECM-repaired muscle

Transplanted mECMs (*with or without BMSCs*) were remodeled and replaced with fibrous tissue (Fig. 6). The laminin staining marking the transplanted mECM at two weeks post-injury (Fig. 2B) was no longer present at prolonged time points (Fig. 6B), indicating a complete remodeling of the mECM. In the area of the defect, a large fibrotic mass composed of collagen I (*and collagen III; data not shown*) appeared to be integrated with the remaining muscle mass (Fig. 6D). In contrast, non-repaired muscles demonstrated an increased collagen I deposition in the remaining muscle mass immediately under the defect area (Fig. 6C). That is to say, non-repaired and mECM repaired muscles presented with fibrosis in distinctly different areas after VML injury. The area fraction of intramuscular collagen I (located exclusively within the remaining muscle mass) was nearly two-fold greater for no repair compared to uninjured, mECM, and mECM + BMSC groups by two months post-injury (17 ± 2 vs. 10 ± 1, 10 ± 1, & 10 ± 1%, respectively; $p < 0.001$). The increased fibrosis in each group, appeared to be associated with a prolonged inflammatory response, as CD68 + cells were localized to the area of fibrosis in each respective tissue (Fig. 6E and F). Stated otherwise, macrophages were located within the remaining muscle mass in non-repaired muscle and primarily limited to the defect area in mECM-treated muscle.

3.4. Functional capacity of non-repaired and mECM-treated muscles

Animal and TA muscle characteristics are listed in Table 1. Active TA muscle isometric tetanic force was measured *in situ* at two, four, or six months post-injury in injured and contralateral uninjured muscles (Fig. 7). Because there were significant differences in body weight among groups at the time of sacrifice, despite weights being similar at the time of surgery (Table 1), maximal isometric forces were normalized to body weight. Following normalization, force produced by contralateral uninjured muscles was similar among groups at each time post-injury and was therefore considered as one group (Table 1). At two and four months post-injury, non-repaired muscles exhibited a −29 and −31% deficit, respectively, compared to uninjured contralateral muscles. At these times (2 and 4 months post-injury), the functional deficit was reduced to −23 and −25% for mECM and −22 and −18% for mECM + BMSC treated muscles. Interestingly, at 6 months post-injury non-repaired muscles exhibited an improved functional capacity resulting in a −20% force deficit − mECM and mECM + BMSC treated muscles maintained a −22 and −18% deficit, respectively. Thus, while mECM-based treatments improved functional recovery over the first four months post-injury, non-repaired muscle exhibited

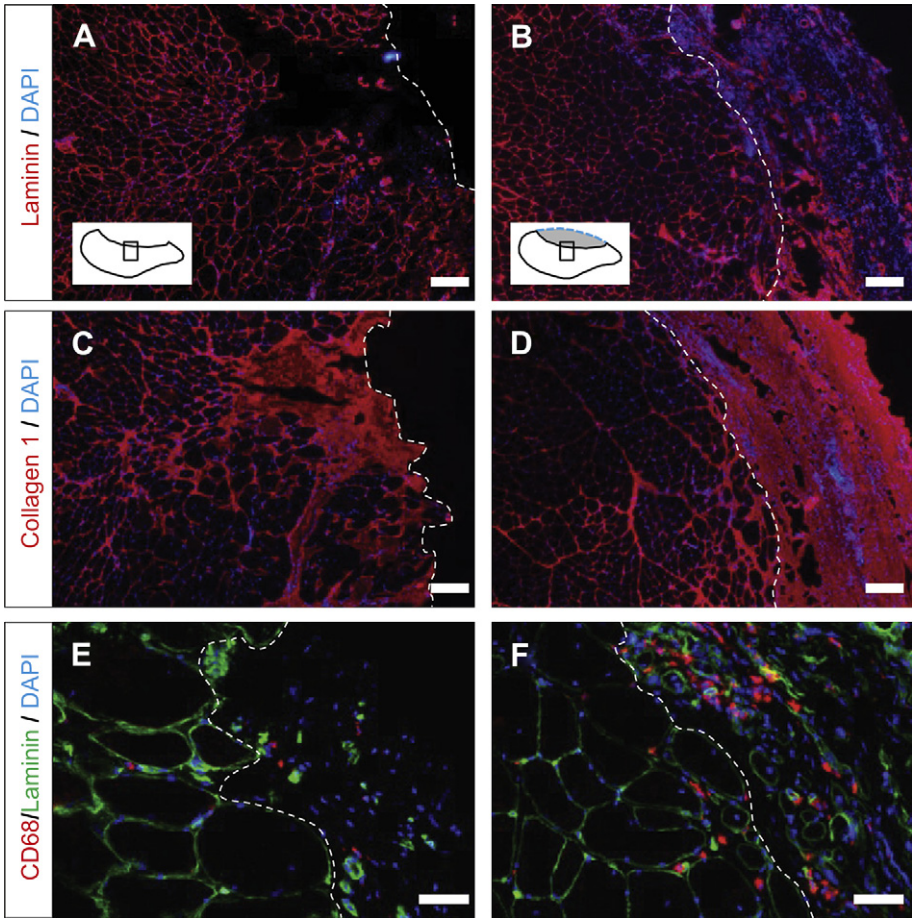

Fig. 6. Scar formation at the site of the defect after volumetric muscle loss injury. TA muscles from no repair (A, C, & E) and mECM-repaired (B, D, & F) groups were harvested two months post-injury and cross-sections of the muscle were fluorescently probed for markers, as denoted on each row of images. *Note*: The diagram of the TA muscle illustrates where the depicted images for each group were captured relative to the defect site. White dashed lines indicate the approximate interface between the remaining muscle mass (left) and transplanted mECM (right). Images A–D are of 40× magnification; Scale bar = 200 μm, while images E & F are 200× magnification; Scare bar = 50 μm.

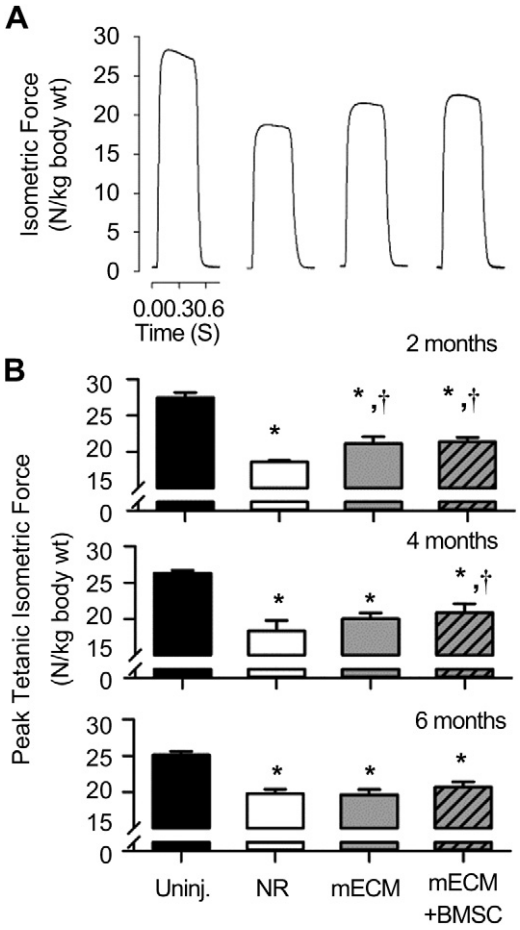

Fig. 7. *In situ* TA muscle isometric force production following volumetric muscle loss injury and repair with tissue engineering strategies. Isometric force was measured in non-repaired (NR), mECM-repaired, and mECM + BMSC repaired muscles 2, 4, and 6 months post-injury using identical neural stimulation parameters described in Fig. 2. Force measured from the contralateral control muscles were used as uninjured controls. Representative force tracings for each group two months post-injury are illustrated (A) and group means ± SEM (sample sizes are listed in Table 1; B) are presented for each time point as listed. Annotated group means are statistically different ($p < 0.05$) from (*) uninjured and (†) non-repaired muscles.

a delayed improvement in force from four to six months post-injury.

3.5. Muscle fiber damage, repair, and remodeling in the remaining muscle mass

Extensive fiber damage and remodeling was observed radiating from the defect area into the remaining muscle mass in non-repaired muscle out to four months post-injury (Fig. 8A and D). Muscles repaired with mECM (with or without BMSC delivery) did not present with this damage to the remaining muscle mass (e.g., Fig. 8B and C), suggesting that the functional improvements observed with mECM transplantation at two and four months post-injury are primarily due to attenuation of damage of the remaining musculature. As further support of this supposition, six months post-injury the non-repaired muscle appeared to remodel and repair the damage observed at earlier time points (Fig. 8G), which coincided with the delayed improvements in force production observed in this group (Fig. 7). Lastly, the mean cross-sectional area of muscle fibers in the remaining muscle mass of non-repaired muscle was significantly less than either mECM treated (with or without BMSCs) and uninjured muscles (Fig. 9), lending further support that mECM-based treatments impact the remodeling processes of the remaining muscle mass after VML.

4. Discussion

There is a growing research effort to develop tissue engineering technologies for the treatment of volumetric muscle loss. The primary treatment outcome for therapies of VML is an improvement in muscle function [15]. To achieve this goal, a large emphasis has been placed on generating functional muscle fibers to replace those that were lost. However, while fiber generation is certainly ideal, there also exists a currently unaddressed opportunity for tissue engineering/regenerative medicine therapies to improve the functional capacity of the remaining muscle mass. Stated otherwise and simply, the functional deficits following VML may not only be due to the frank loss of tissue, but may also involve changes in muscle architecture [41], dampened force transmission [42,43], and prolonged muscle damage [14] to the remaining portion of injured muscle. This is effectively demonstrated in preclinical VML models by the fact that the functional deficit of non-repaired muscle is greater in magnitude than the mass of tissue excised [9,10,13,20]. Thus, there is ample opportunity to make incremental improvements in function after VML by not only generating neo-tissue, but also by improving the functional efficiency and capacity of the remaining musculature.

The results of this study demonstrate that a skeletal muscle derived biological ECM without the addition of a stem or progenitor cell source can enhance the rate of functional recovery of VML injured muscle, and that this improved rate of recovery may be due to improvements in the remaining muscle mass. This is the first study to demonstrate such an effect on a whole muscle level under *in vivo* conditions (i.e., neural stimulation with the muscle remaining under endogenous blood supply). In part, the findings of the current study agree with previous reports indicating that biological ECM-mediated improvements in function using non-classical physiological assessments [22,30], but disagrees with other related studies [10,20]. To this end, the current findings support that biological ECM-based therapies meet the basic criteria of a successful treatment for VML – that is an improvement in functional recovery of the injured musculature [15].

Given the lack of muscle fiber generation observed within the defect area in the current study, the functional improvements observed at two and four months post-injury following mECM transplantation (with or without BMSC injection) cannot be explained even partly by the generation of functional tissue, unlike other related studies [9,20–22,30]. Instead of muscle fibers, a large fibrotic mass (laminincollagen I positive; Fig. 6) was observed by two months post-injury in the area where the mECM (laminin + at two weeks; Fig. 2) was transplanted; findings that are in agreement to those presented previously by Turner et al. [44], and Gamba et al. [45] following transplantation of xenogenic SIS scaffold or syngeneic mECM, respectively. In fact, there is disparity among studies describing the ability of biological scaffolds (*with or without the inclusion of stem or progenitor cells*) to generate a clinically relevant volume of skeletal muscle fibers in VML or VML-like (*abdominal wall*) models. In many reports, a modest level of muscle fiber generation is demonstrated [9,20,21,23,30], although there are also more extreme examples of an abundance [22,24] and a dearth [44,45] of muscle fiber generation following ECM transplantation. Regardless of the final outcome (i.e., muscle fiber generation vs. fibrosis) or specific tissue engineering approach used (i.e., type of ECM, inclusion/specific cell source), significant collagen deposition is consistently observed in the area of the transplant at least intermittently post-transplantation [e.g., Ref. [22]].

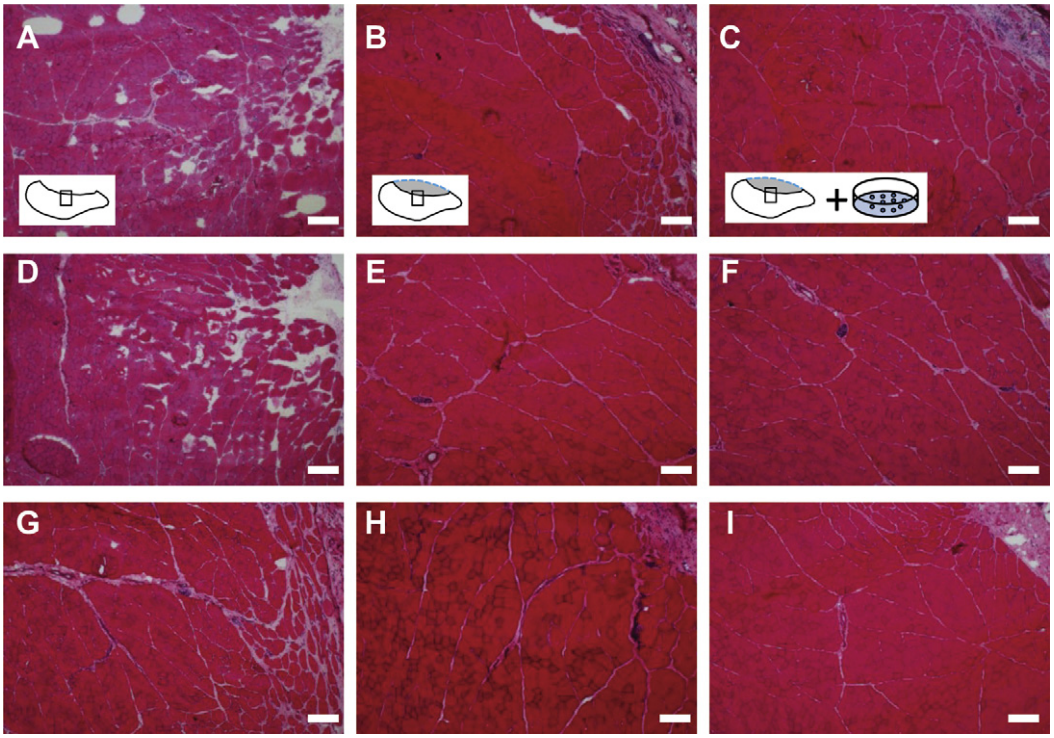

Fig. 8. Prolonged muscle fiber damage and disruption in the remaining muscle mass following volumetric muscle loss. TA muscles from no repair (A, D, & G), mECM-repaired (B, E, & H), and mECM + BMSC repaired (C, F, & I) were harvested at 2 (A–C), 4 (D–F), or 6 (G–I) months post-injury and stained. Cross-sections were stained with hematoxylin and eosin. *Note*: The diagram of the TA muscle illustrates where the depicted images for each group were captured relative to the defect site. Images are of 40× magnification; Scale bar = 200 μm.

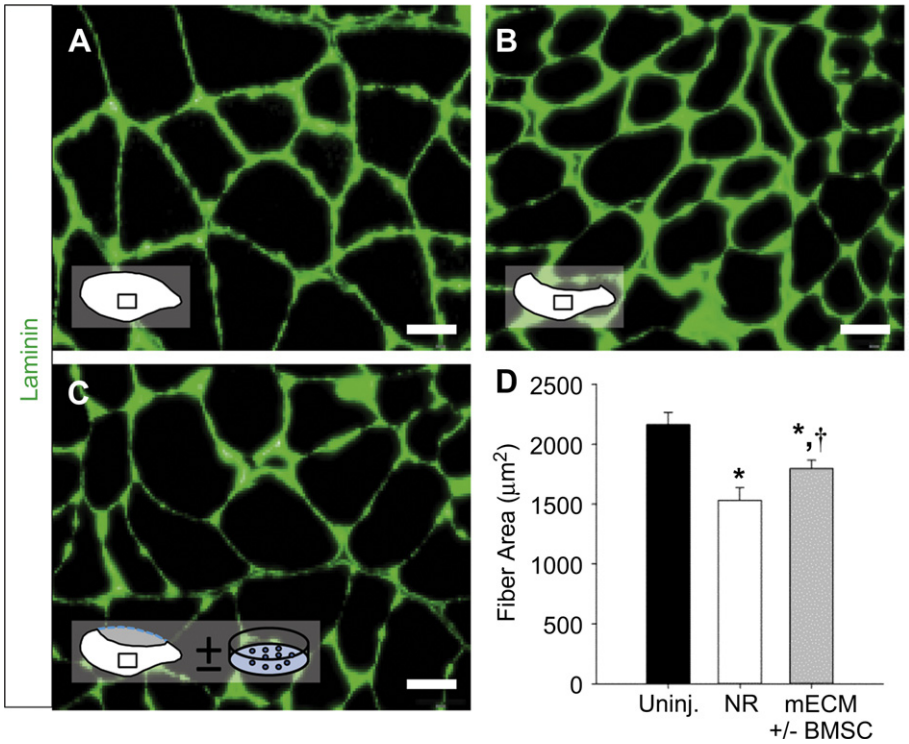

Fig. 9. Architectural alterations of the remaining muscle mass after volumetric muscle loss. Contralateral uninjured (A; $n = 5$) and VML injured non-repaired (B; $n = 9$) and mECM-repaired with or without BMSC (C; $n = 18$) muscles were harvested at 2, 4 and 6 months post-injury. Muscle fiber area was measured for fibers located in the remaining muscle mass from laminin stained sections (A–D) using a custom written macro in Image J. Images are 200× magnification; Scale bar = 50 μm. Group fiber area means ± SEM (D) are presented for all time points combined. Annotated group means are statistically different ($p < 0.05$) from (*) uninjured and (†) non-repaired muscles.

With this in mind, the current findings point towards a novel mechanism by which biological ECMs may improve the functional capacity of skeletal muscle with VML, wherein the commonly observed ECM-mediated collagen deposition in the defect area treats the remaining muscle mass. In support, we observed an association between the timing of endogenous healing (non-repaired) and prevention (mECM-repaired) of prolonged muscle fiber damage in the remaining muscle mass with the partial restoration of functional capacity over the course of six months post-injury (Figs. 7 and 8). Additionally, we observed that mECM transplantation partially prevented reductions in fiber cross-sectional area in the remainder of VML injured muscle (Fig. 9), indicating attenuation of either muscle fiber atrophy or a reduction in fiber pennation angle [46]. Collectively these findings support the supposition that mECM directed collagen deposition within the defect area protects the remaining musculature from prolonged muscle damage and potentially muscle fiber atrophy, and in doing so incrementally improves the rate of recovery of net force production.

Very little is currently understood regarding the response of the remaining muscle mass after VML. Presumably VML results in vascular and neural damage and muscle fiber injury, all with the potential to induce an ensuing inflammatory response and fibrosis. Additionally, mechanical overload induces further injury upon restoration of use of the muscle or muscle unit, as occurs with synergist muscle ablation [47] and with the myopathology of dystrophic mice [48,49]. In fact, the prolonged (~4–6 months) presence of muscle damage in the remaining muscle is suggestive of the repeated cycles of muscle fiber degeneration and regeneration that are a hallmark of muscular dystrophy [49], raising concerns as to whether the regenerative capacity of the remaining muscle mass may become diminished [50,51] following a prolonged period of endogenous healing [8]. The extent of mechanical overload injury secondary to VML, is likely determined by the magnitude and frequency of stress placed on the remaining tissue [52,53] and thus is dependent on VML injury severity (e.g., 20 vs 60% of the tissue remaining) as well as muscle activity, among other factors (e.g., type of muscle injured). Given the location (i.e., radiating inward from the defect area into the remaining muscle mass), we presume that the prolonged muscle damage observed in non-repaired muscles two and four months post-injury (Fig. 8) is the result of chronic overload, wherein the defect area is most vulnerable to greater relative mechanical stress. In this scenario, the increased collagen deposition mediated by mECM transplantation [42,43,54], may have served as structural reinforcement for the underlying fibers and/or as a fibrous network serving to transmit forces, an apparent conserved response of skeletal muscle to increased mechanical stress (e.g., desmin knockout mice [36], repeated strain injury [55,56], & biceps muscle injury [57]). Additionally, degradation of the mECM may have also released trophic factors capable of assisting regeneration of the remaining muscle mass. Ultimately, in this VML model the result of mECM-mediated collagen deposition within the area of the defect is a clear attenuation of prolonged fiber damage and putative atrophy within the remaining muscle mass.

Undoubtedly, the primary goal of tissue engineering therapies for VML is to improve functional capacity *in vivo*, by promoting the generation of new muscle fibers to replace those that were lost. In this study, we demonstrate that transplantation of a biological ECM can improve the rate of muscle force recovery without significant muscle fiber generation. Instead, the extensive mECM mediated collagen deposition appeared to protect the remaining muscle mass from prolonged muscle injury and fibrosis. However, it should be noted that, in this model, the magnitude of functional recovery promoted by mECM transplantation (with or without the inclusion of BMSCs) was eventually met, albeit four months later, by endogenous repair mechanisms. On one hand, this highlights the absolute requirement for tissue engineering therapies to promote significant muscle fiber generation in order to significantly improve functional recovery. On the other hand, the formation of functional fibrosis alone in the defect area may attenuate the progression of a chronic intramuscular fibrosis, while at the same time potentially allowing for greater treatment efficacy with physical rehabilitation (i.e., the muscle can withstand greater mechanical stress). Under most circumstances, the current tissue engineering paradigm appears to provide both an initial collagen deposition and then later, an increased presence of putative functional muscle fibers in the defect area, suggesting that both mechanisms of functional recovery explain the findings of previous reports [e.g., Ref. [22]].

Clearly, there remain questions regarding optimal treatment strategies for VML, not the least of which is the optimal timing for treatment. Currently, no animal model of VML has been given a delayed treatment (i.e., months after injury), whereas, the only clinical report of a tissue engineering device used to treat VML was ~3 years post-injury [8]. Future animal studies investigating the role of tissue engineering solutions (including biological ECMs with and without stem or progenitor cells) for VML should begin to consider the clinical realities of comorbidities (e.g., bone fracture [13]), treatment timing (e.g., acute vs. delayed), and concomitant therapies (e.g., physical rehabilitation).

Lastly, it is important to emphasize that the finding of the current study, that mECM with and without BMSC injection does not promote muscle fiber generation, is limited to the specific conditions of this study and should be interpreted broadly with caution. Biological ECM preparation (i.e., decellularization) procedures can vary in the degree of cellular removal, disruption of the ultrastructure, and deterioration of biological activity [23,37], and therefore have a profound impact on *in vivo* ECM performance. We cannot currently explain why the mECM (prepared with minor variations to Stern et al. [31]) in the current study did not support muscle fiber generation, when 1) the ECM was sufficiently decellularized but still maintained biological factors capable of promoting muscle progenitor cell proliferation (Figs. 1 and 2) other mECMs have been shown to promote a low level of fiber generation *in vivo* using potentially harsher [10,21] and gentler [23] preparations. Similarly, it is difficult to reconcile why the delayed injection of BMSCs did not promote tissue generation in the defect area, as our lab group has demonstrated previously [21]. While these discrepant findings may be related to differences among biological scaffolds, they may also be due to different injury models (TA muscle vs. lateral gastrocnemius muscle [21]) employed. In support of the latter, recently the Badylak laboratory demonstrated that transplantation of SIS-based ECMs promoted the generation of a remarkable volume of skeletal muscle fibers in a muscle-tendon injury [22], but extensive fibrosis in a complex quadriceps muscle injury in dogs [44]. Collectively, discrepancies within the related literature and with this study broadly indicate that a variety of tissue engineering solutions are likely required to provide personalized care for civilians and Wounded Warriors with VML.

5. Conclusion

The salient finding of this study is that a biological ECM can improve the functional capacity of skeletal muscle with VML by increasing the mechanical stability (i.e., lessening prolonged muscle damage) of the remaining muscle mass. This points to a novel role of biological ECM transplantation indicating that while prolonged regenerative events occur, the commonly observed collagen deposition in the defect may have beneficial therapeutic outcomes directed at the remaining musculature. These are encouraging

findings for developing tissue engineering strategies using biological ECMs, especially in the context of combining the effects of physical rehabilitation and tissue engineering therapies.

Acknowledgments

We would like to thank Mrs. Janet Roe,Ms. Melissa Sanchez, and Dr. Kelly Chen for their technical support of this work. Additionally, we thank Dr. Ramon Coronado for his assistance in preparing the milled mECM and Dr. Amit Aurora for his insightful discussion of the findings. This work was funded by the U.S. Army Medical Research and Medical Command (grants: W81XWH-09-2-0177 and F_013-2010-USAISR) awarded to TJW. All components of this study including the decision where to publish were of the sole discretion of the authors. The opinions or assertions contained herein are the private views of the authors and are not to be construed as official or reflecting the views of the Department of Defense (AR 360-5) or the United States Government. The authors are employees of the U.S. government and this work was prepared as part of their official duties.

References

[1] Lepper C, Partridge TA, Fan CM. An absolute requirement for pax7-positive satellite cells in acute injury-induced skeletal muscle regeneration. Development 2011;138:3639–46.
[2] Rathbone CR, Wenke JC, Warren GL, Armstrong RB. Importance of satellite cells in the strength recovery after eccentric contraction-induced muscle injury. Am J Physiol Regul Integr Comp Physiol 2003;285:R1490–5.
[3] Caldwell CJ, Mattey DL, Weller RO. Role of the basement membrane in the regeneration of skeletal muscle. Neuropathol Appl Neurobiol 1990;16:225–38.
[4] Maltin CA, Harris JB, Cullen MJ. Regeneration of mammalian skeletal muscle following the injection of the snake-venom toxin, taipoxin. Cell Tissue Res 1983;232:565–77.
[5] Warren GL, Hulderman T, Mishra D, Gao X, Millecchia L, O'Farrell L, et al. Chemokine receptor ccr2 involvement in skeletal muscle regeneration. FASEB J 2005;19:413–5.
[6] Tidball JG. Inflammatory processes in muscle injury and repair. Am J Physiol Regul Integr Comp Physiol 2005;288:R345–53.
[7] Lin CH, Lin YT, Yeh JT, Chen CT. Free functioning muscle transfer for lower extremity posttraumatic composite structure and functional defect. Plast Reconstr Surg 2007;119:2118–26.
[8] Mase Jr VJ, Hsu JR, Wolf SE, Wenke JC, Baer DG, Owens J, et al. Clinical application of an acellular biologic scaffold for surgical repair of a large, traumatic quadriceps femoris muscle defect. Orthopedics 2010;33:511.
[9] Corona BT, Machingal MA, Criswell T, Vadhavkar M, Dannahower AC, Bergman C, et al. Further development of a tissue engineered muscle repair construct in vitro for enhanced functional recovery following implantation in vivo in a murine model of volumetric muscle loss injury. Tissue Eng Part A 2012;18:1213–28.
[10] Merritt EK, Hammers DW, Tierney M, Suggs LJ, Walters TJ, Farrar RP. Functional assessment of skeletal muscle regeneration utilizing homologous extracellular matrix as scaffolding. Tissue Eng Part A 2010;16:1395–405.
[11] Shi M, Ishikawa M, Kamei N, Nakasa T, Adachi N, Deie M, et al. Acceleration of skeletal muscle regeneration in a rat skeletal muscle injury model by local injection of human peripheral blood-derived cd133-positive cells. Stem Cells 2009;27:949–60.
[12] Tamaki T, Uchiyama Y, Okada Y, Ishikawa T, Sato M, Akatsuka A, et al. Functional recovery of damaged skeletal muscle through synchronized vasculogenesis, myogenesis, and neurogenesis by muscle-derived stem cells. Circulation 2005;112:2857–66.
[13] Willett NJ, Li MT, Uhrig BA, Boerckel JD, Huebsch N, Lundgren TL, et al. Attenuated human bone morphogenetic protein-2-mediated bone regeneration in a rat model of composite bone and muscle injury. Tissue Eng Part C Methods. http://dx.doi.org/10.1089/ten.TEC.2012.0290. Available from: http://www.ncbi.nlm.nih.gov/pubmed/22992043; 2012.
[14] Wu X, Corona BT, Chen X, Walters TJ. A standardized rat model of volumetric muscle loss injury for the development of tissue engineering therapies. BioRes Open Access 2012;1:280–90.
[15] Grogan BF, Hsu JR. Volumetric muscle loss. J Am Acad Orthop Surg 2011;19(Suppl. 1):S35–7.
[16] Studitsky AN. Free auto- and homografts of muscle tissue in experiments on animals. Ann N Y Acad Sci 1964;120:789–801.
[17] Carlson BM. Regeneration of the completely excised gastrocnemius muscle in the frog and rat from minced muscle fragments. J Morphol 1968;125:447–72.
[18] Carlson BM. The regeneration of a limb muscle in the axolotl from minced fragments. Anat Rec 1970;166:423–34.
[19] Carlson BM, Gutmann E. Development of contractile properties of minced muscle regenerates in the rat. Exp Neurol 1972;36:239–49.
[20] Machingal MA, Corona BT, Walters TJ, Kesireddy V, Koval CN, Dannahower A, et al. A tissue-engineered muscle repair construct for functional restoration of an irrecoverable muscle injury in a murine model. Tissue Eng Part A 2011;17:2291–303.
[21] Merritt EK, Cannon MV, Hammers DW, Le LN, Gokhale R, Sarathy A, et al. Repair of traumatic skeletal muscle injury with bone-marrow-derived mesenchymal stem cells seeded on extracellular matrix. Tissue Eng Part A 2010;16:2871–81.
[22] Turner NJ, Yates Jr AJ, Weber DJ, Qureshi IR, Stolz DB, Gilbert TW, et al. Xenogeneic extracellular matrix as an inductive scaffold for regeneration of a functioning musculotendinous junction. Tissue Eng Part A 2010;16:3309–17.
[23] Wolf MT, Daly KA, Reing JE, Badylak SF. Biologic scaffold composed of skeletal muscle extracellular matrix. Biomaterials 2012;33:2916–25.
[24] De Coppi P, Bellini S, Conconi MT, Sabatti M, Simonato E, Gamba PG, et al. Myoblast-acellular skeletal muscle matrix constructs guarantee a long-term repair of experimental full-thickness abdominal wall defects. Tissue Eng 2006;12:1929–36.
[25] Gulati AK. Basement membrane component changes in skeletal muscle transplants undergoing regeneration or rejection. J Cell Biochem 1985;27:337–46.
[26] Valentin JE, Stewart-Akers AM, Gilbert TW, Badylak SF. Macrophage participation in the degradation and remodeling of extracellular matrix scaffolds. Tissue Eng Part A 2009;15:1687–94.
[27] Agrawal V, Tottey S, Johnson SA, Freund JM, Siu BF, Badylak SF. Recruitment of progenitor cells by an extracellular matrix cryptic peptide in a mouse model of digit amputation. Tissue Eng Part A 2011;17:2435–43.
[28] Badylak SF, Valentin JE, Ravindra AK, McCabe GP, Stewart-Akers AM. Macrophage phenotype as a determinant of biologic scaffold remodeling. Tissue Eng Part A 2008;14:1835–42.
[29] Perniconi B, Costa A, Aulino P, Teodori L, Adamo S, Coletti D. The pro-myogenic environment provided by whole organ scale acellular scaffolds from skeletal muscle. Biomaterials 2011;32:7870–82.
[30] Valentin JE, Turner NJ, Gilbert TW, Badylak SF. Functional skeletal muscle formation with a biologic scaffold. Biomaterials 2010;31:7475–84.
[31] Stern MM, Myers RL, Hammam N, Stern KA, Eberli D, Kritchevsky SB, et al. The influence of extracellular matrix derived from skeletal muscle tissue on the proliferation and differentiation of myogenic progenitor cells ex vivo. Biomaterials 2009;30:2393–9.
[32] Allen RE, Temm-Grove CJ, Sheehan SM, Rice G. Skeletal muscle satellite cell cultures. Methods Cell Biol 1997;52:155–76.
[33] Kragh Jr JF, Svoboda SJ, Wenke JC, Ward JA, Walters TJ. Suturing of lacerations of skeletal muscle. J Bone Joint Surg Br 2005;87:1303–5.
[34] Wu X, Wolf SE, Walters TJ. Muscle contractile properties in severely burned rats. Burns 2010;36:905–11.
[35] Wu X, Baer LA, Wolf SE, Wade CE, Walters TJ. The impact of muscle disuse on muscle atrophy in severely burned rats. J Surg Res 2010;164:e243–51.
[36] Meyer GA, Lieber RL. Skeletal muscle fibrosis develops in response to desmin deletion. Am J Physiol Cell Physiol 2012;302:C1609–20.
[37] Crapo PM, Gilbert TW, Badylak SF. An overview of tissue and whole organ decellularization processes. Biomaterials 2011;32:3233–43.
[38] Engler AJ, Sen S, Sweeney HL, Discher DE. Matrix elasticity directs stem cell lineage specification. Cell 2006;126:677–89.
[39] Valero MC, Huntsman HD, Liu J, Zou K, Boppart MD. Eccentric exercise facilitates mesenchymal stem cell appearance in skeletal muscle. PLoS One 2012;7:e29760.
[40] Matziolis G, Winkler T, Schaser K, Wiemann M, Krocker D, Tuischer J, et al. Autologous bone marrow-derived cells enhance muscle strength following skeletal muscle crush injury in rats. Tissue Eng 2006;12:361–7.
[41] Ward SR, Sarver JJ, Eng CM, Kwan A, Wurgler-Hauri CC, Perry SM, et al. Plasticity of muscle architecture after supraspinatus tears. J Orthop Sports Phys Ther 2010;40:729–35.
[42] Purslow PP. The structure and functional significance of variations in the connective tissue within muscle. Comp Biochem Physiol A Mol Integr Physiol 2002;133:947–66.
[43] Purslow PP. Muscle fascia and force transmission. J Bodyw Mov Ther 2010;14:411–7.
[44] Turner NJ, Badylak JS, Weber DJ, Badylak SF. Biologic scaffold remodeling in a dog model of complex musculoskeletal injury. J Surg Res 2012;176:490–502.
[45] Gamba PG, Conconi MT, Lo Piccolo R, Zara G, Spinazzi R, Parnigotto PP. Experimental abdominal wall defect repaired with acellular matrix. Pediatr Surg Int 2002;18:327–31.
[46] Gollnick PD, Timson BF, Moore RL, Riedy M. Muscular enlargement and number of fibers in skeletal muscles of rats. J Appl Physiol 1981;50:936–43.
[47] Tamaki T, Akatsuka A, Tokunaga M, Uchiyama S, Shiraishi T. Characteristics of compensatory hypertrophied muscle in the rat: I. Electron microscopic and immunohistochemical studies. Anat Rec 1996;246:325–34.
[48] Brussee V, Tardif F, Tremblay JP. Muscle fibers of mdx mice are more vulnerable to exercise than those of normal mice. Neuromuscul Disord 1997;7:487–92.
[49] Pastoret C, Sebille A. Mdx mice show progressive weakness and muscle deterioration with age. J Neurol Sci 1995;129:97–105.

[50] McGeachie JK, Grounds MD, Partridge TA, Morgan JE. Age-related changes in replication of myogenic cells in mdx mice: quantitative autoradiographic studies. J Neurol Sci 1993;119:169–79.
[51] Lund TC, Grange RW, Lowe DA. Telomere shortening in diaphragm and tibialis anterior muscles of aged mdx mice. Muscle Nerve 2007;36:387–90.
[52] Warren GL, Hayes DA, Lowe DA, Armstrong RB. Mechanical factors in the initiation of eccentric contraction-induced injury in rat soleus muscle. J Physiol 1993;464:457–75.
[53] Warren GL, Hayes DA, Lowe DA, Prior BM, Armstrong RB. Materials fatigue initiates eccentric contraction-induced injury in rat soleus muscle. J Physiol 1993;464:477–89.
[54] Lehto M, Duance VC, Restall D. Collagen and fibronectin in a healing skeletal muscle injury. An immunohistological study of the effects of physical activity on the repair of injured gastrocnemius muscle in the rat. J Bone Joint Surg Br 1985;67:820–8.
[55] Stauber WT, Knack KK, Miller GR, Grimmett JG. Fibrosis and intercellular collagen connections from four weeks of muscle strains. Muscle Nerve 1996; 19:423–30.
[56] Stauber WT, Smith CA, Miller GR, Stauber FD. Recovery from 6 weeks of repeated strain injury to rat soleus muscles. Muscle Nerve 2000;23:1819–25.
[57] Kragh Jr JF, Basamania CJ. Surgical repair of acute traumatic closed transection of the biceps brachii. J Bone Joint Surg Am 2002;84-A:992–8.